Influence of Helicopter Rotor Wake Modeling on Blade Airload Predictions

Christos K. Zioutis zioutis@mech.upatras.gr
Mechanical Engineering and Aeronautics Department University of Patras Rio Patras, 26500, Greece

Apostolos I. Spyropoulos spyrop@mech.upatras.gr
Mechanical Engineering and Aeronautics Department University of Patras Rio Patras, 26500, Greece

Anastasios P. Fragias fragias@mech.upatras.gr
Mechanical Engineering and Aeronautics Department University of Patras Rio Patras, 26500, Greece

Dionissios P. Margaris margaris@mech.upatras.gr
Mechanical Engineering and Aeronautics Department University of Patras Rio Patras, 26500, Greece

Dimitrios G. Papanikas papanikas@mech.upatras.gr
Mechanical Engineering and Aeronautics Department University of Patras Rio Patras, 26500, Greece

Abstract

In the present paper a computational investigation is made about the efficiency of recently developed mathematical models for specific aerodynamic phenomena of the complicated helicopter rotor flowfield. A developed computational procedure is used, based on a Lagrangian type, Vortex Element Method. The free vortical wake geometry and rotor airloads are computed. The efficiency of special models concerning vortex core structure, vorticity diffusion and vortex straining regarding rotor airloads prediction is tested. Investigations have also been performed in order to assess a realistic value for empirical factors included in vorticity diffusion models. The benefit of using multiple vortex line to simulate trailing wake vorticity behind blade span instead of isolated lines or vortex sheets, despite their computational cost, is demonstrated with the developed wake relaxation method. The computational results are compared with experimental data from wind tunnel tests, performed during joined European research programs.

Keywords: Helicopter aerodynamics, rotor wake, vortex core.

1. INTRODUCTION

Computational research on helicopter rotors focuses on blade airloads prediction, trying to identify the effects of important operational, structural and flowfield parameters such as wake formation, blade planform, flight conditions etc on blade vibrations and noise emissions. Improved helicopter performance is a continuous research challenge as aeronautical industry is always seeking for a more efficient, vibration free and "quiet" rotorcraft with increased public acceptance.

The main issue in helicopter aerodynamics examined by many computational and experimental efforts is the interaction of rotor blades with wake vortices, a phenomenon which characterizes helicopters and is the source of blade vibration and noise emission. As in other similar aerodynamic flowfields, such as the trailing wake of aircrafts or wind turbines, the velocity field in the vicinity of a helicopter rotor must be calculated from the vorticity field. A prerequisite for such a calculation is that the physical structure and the free motion of wake vortices are adequately simulated.

Vortex Element Methods (VEM) have been established during recent years computational research as an efficient and reliable tool for calculating the velocity field of concentrated three-dimensional, curved vortices [1,2]. Wake vortices are considered as vortex filaments which are free to move in Lagrangian coordinates. The filaments are descritized into piecewise segments and a vortex element is assigned to each one of them. Since the flow is considered inviscid except for the vortices themselves, the Biot-Savart low is applied in closed-form integration over each vortex element for the velocity field calculation. Marked points are traced on vortex filaments as they move freely due to the mutual-induced velocity field, either by externally imposing geometrical periodicity (relaxation methods) or not (time marching methods). Thus, VEM can computationally reproduce an accurate geometry of the concentrated wake vortices spinning close to rotor disk. As a result the non-uniform induced downwash of lifting helicopter rotors can be computed, which is responsible for rotor blade vibratory airloads.

From the first simplified approaches [3,4], to recent advanced procedures [5-9], the vorticity elements used are vortex lines and vortex sheets [5,10]. The sophistication level of rotor wake analysis can vary from preliminary to advanced manufacture calculations. The basic formulation of VEM is closely related to classical vortex methods for boundary layer and vortical flow analysis extensively applied by Chorin [11], Leonard [12] and other researchers [13,33].

The extensive effort made by a number of researchers has resulted to several models proposed for simulating viscous vortex core structure, vorticity diffusion, trailing vortex rollup process, rotor blade dynamic stall and other phenomena [14]. These different physico-mathematical models have a significant influence on computed blade airload distributions, while their reliability for the majority of helicopter rotor flow conditions is always under evaluation.

The contribution of the work presented here is to investigate the influence of specific aerodynamic models on computed blade airloads, evaluating their reliability by comparisons of computed results with experimental data. In addition, the values of empirical factors included in these models are computationally verified. The applied method consists of a free wake analysis, using a wake-relaxation type VEM [15,16,29] and a coupled airload computation module which has the flexibility to adopt either lifting line or lifting surface methods. Blade motion calculations include provisions for articulated or hingeless blades and the main rigid and elastic flapping modules can be regarded separately or coupled.

When helicopter rotor wakes are simulated, then the line segment discretization of wake vortices is prevailed. Methods with straight [8,10] or curved [6,17] line segments have been proposed and their accuracy was found to be of second order comparing to vortex ring analytical solution [18,19]. Rarely, the distributed vorticity behind the inner part of blade span is modeled by surface elements such as vortex sheets [10]. For the present investigation, a model of multiple trailing lines is adopted and compared with models of simpler discretization.
Viscous effects on wake vorticity have also been the subject of computational and experimental efforts because of their significant impact on induced velocity calculations especially for large wake ages [20-22]. These effects are the vortex core formation in the center of vortex lines and the diffusion of the concentrated vorticity as time progresses. Both of these phenomena are found to be of crucial importance for a reliable wake representation. In the present paper several models are compared, assuming both laminar and turbulent vortex core flow, in order to demonstrate their effectiveness and a parametric investigation is performed concerning empirical factors employed by these models.

The experimental data used for comparisons include test cases executed during cooperative European research programs on rotorcraft aerodynamics and aeroacoustics performed in the open test section of the German-Dutch Wind Tunnel (DNW) The Netherlands [23].

2. AERODYNAMIC FORMULATION

2.1 Rotor Wake Model

The vorticity generated in rotor wake is distinguished regarding its source in two main parts, the trailing and the shed vorticity. Conservation of circulation dictates that the circulation gradients on a rotor blade determine the vorticity shed at specific spanwise locations behind the blade. Thus spanwise circulation variations generate trailing vorticity, g_n, whose direction is parallel to the local flow velocity (Figure 1). On the other hand, azimuthal variations produce shed vorticity radially oriented, g_s, due to the transient periodical nature of the rotor blade flowfield. In general, bound circulation has a distribution as shown in Figure 1, where the pick is located outboard of the semi-span and a steep gradient appears closely to blade tip. This gradient generates a high strength trailing vortex sheet just behind the blade which quickly rolls up and forms a strong tip vortex.

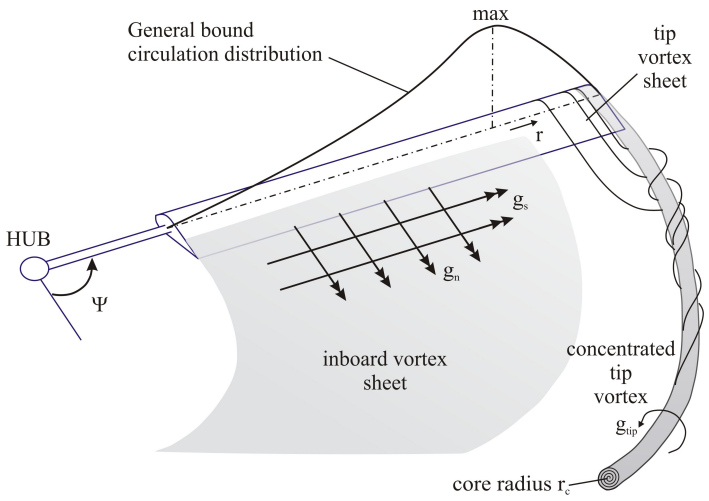

FIGURE 1: Rotor wake physicomathematical modeling.

The continuous distribution of wake vorticity shown in Figure 1 is discretized into a series of vortex elements. Depending on the degree of analysis of wake flowfield and on targeted computational consumption, some VEMs use simple disretization as shown in Figure 2. In this

case, bound circulation is assumed as a linearized distribution, as shown in the figure. According to such an assumption, trailing vorticity emanates from the inner part of blade span and is modeled with vortex sheets extending from A to C. Shed vorticity is modeled either with vortex sheets extending from B to E or with vortex lines parallel to blade span as shown in Figure 2. Vortex line discretization is used for tip vortex, except for the area just behind the blade where a rolling up vortex sheet is used. Roll up is simulated with diminishing vortex sheets together with line segments of correspondingly increasing circulation. This type of discretization simulates the basic features of rotor wake with acceptable accuracy and reduces computational consumption especially when VEMs are used in conjunction with CFD simulations of rotor wake in hybrid schemes.

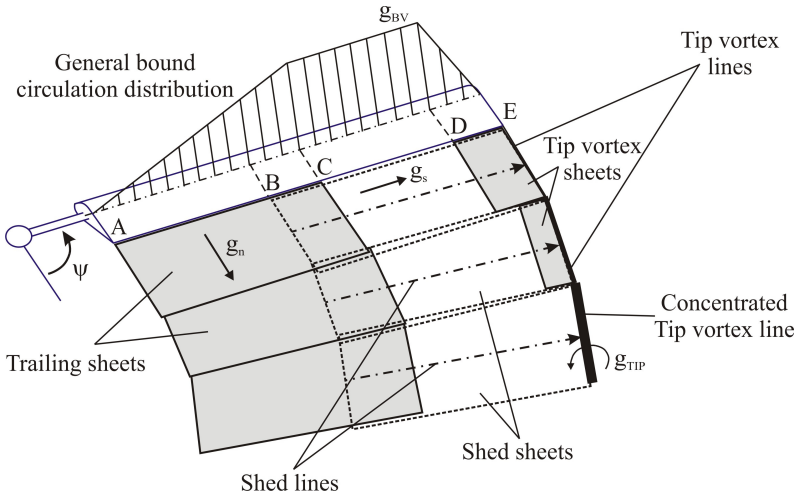

FIGURE 2: Rotor wake simulation, where the trailing wake is represented by vortex sheets, the shed wake either by vortex sheets or vortex lines and the concentrated tip vortex by vortex lines.

Despite the computational efficiency of the above approach, the simplification made in bound circulation distribution can lead to unrealistic results for certain blade azimuth angles. For example, in the cases of reverse flow regions or low advance ratios, where the air hits the rotor blades at the trailing edge or when the rotor blades cut the concentrated tip vortices respectively, a phenomenon known as Blade Vortex Interaction (BVI) is apparent. In these cases the bound circulation distribution departs from the form of Figure 2 and a more detailed discretization is needed in order to catch the specific circulation variations.

In this work, the wake vorticity is discretized in a multitude of trailing and shed vortex lines as shown in Figure 3, in order to simulate the bound circulation distribution in a way that takes into account the fluctuations produced in the majority of blade azimuth angles.

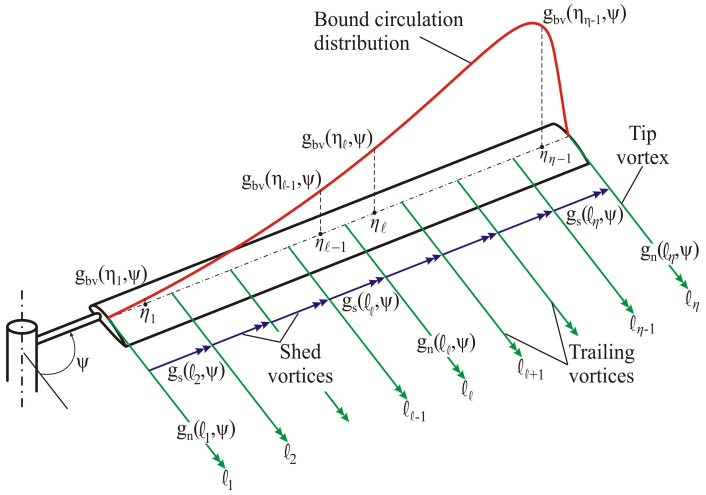

FIGURE 3: Modeling of rotor blade bound circulation distribution and wake vorticity formations with multiple vortex lines.

Trailing vorticity is simulated by n-straight line vortex segments, labeled ℓ_ℓ, which run from ℓ_1 at the root to ℓ_n at the tip. There are η_ℓ=n-1 radial stations where bound circulation is computed, where η_ℓ runs from η_1 between ℓ_1 and ℓ_2 to η_{n-1} between ℓ_{n-1} and ℓ_n. The strength of each segment is equal to the gradient of the bound circulation g_{bv} between two successive radial stations. This means that for all intermediate segments at azimuthal angle ψ:

$$g_n(\ell_\ell,\psi) = g_{bv}(\eta_{\ell-1},\psi) - g_{bv}(\eta_\ell,\psi) \tag{1}$$

The first term is equal to zero at the root because there is no bound circulation inboard the root. Analogically the second term is zero at the tip. The shed vorticity is simulated by n-1 straight line vortex segments which are extended radially between two adjacent trailing vortices as shown in Figure 3. The strength of each segment is equal to the azimuthal variation of bound circulation for each radial station:

$$g_s(\ell_\ell,\psi) = g_{bv}(\eta_{\ell-1},\psi+\Delta\psi) - g_{bv}(\eta_{\ell-1},\psi) \tag{2}$$

where Δψ is the azimuthal step. A number of 50 trailing and shed vortex line segments per azimuthal step were found adequate to discretize the wake vorticity. More detailed discretization will increase computational cost without any tangible improvement of accuracy.

2.2 Induced Velocity Calculation

The distortion of the initial helical geometry of the rotor wake vortices, makes the calculation of the rotor downwash almost impossible with direct numerical integration of the Biot-Savart law, over the actual wake geometry. This procedure is used only for simplified approaches such as the rigid or semi-rigid wake assumptions [3,4]. The utilization of discrete computational elements (vortex lines and sheets) by VEM, converts direct integration in a closed form integration of the Biot-Savart law over the known spatial locations of these elements. The contribution of a vortex line segment i to the induced velocity $\vec{w}_{ij}$ at an arbitrary point in space j, is given by the relation

$$\vec{w}_{ij} = -\frac{1}{4\pi}\int \frac{g_i\left(\vec{r}_{ijm} - k\cdot\vec{e}_k\right)\times d\vec{k}}{\left|\vec{r}_{ijm} - k\cdot\vec{e}_k\right|^3} \tag{3}$$

where $\vec{r}_{ijm}$ is the minimum distance from vortex line i to the point j, $\vec{e}_k$ the unit vector in the direction of the vortex segment, g_i the circulation strength of the vortex segment and k the coordinate measured along the vortex segment. With a reasonable step of discretization, the simplification made to the actual wake geometry can be overcome. After computational investigation the azimuthal step for realistic rotor wake simulations has been proposed by different researchers to be from 2 to 5 degrees [5,32]. The calculation of velocity induced by vortex sheet can be found in [15].

Free vortical wake computation is an iterative procedure, which initiates from rigid wake geometry. Each iteration defines a new position of each vortex element, and takes into account the contribution of all the wake elements to the local flow velocity. At the end of each iteration a new distorted wake geometry is calculated, which is the starting point for the next cycle. This scheme continues until distortion convergence is achieved.

Rotor blade dynamics influence the angle of attack distribution seen by the blade, and therefore alter the bound circulation distribution. Due to out-of-plane motion, rotor blade balances the asymmetry of rotor disk loading. For studying rotor aerodynamics, blade flapwise bending can be represented by a simple mode shape, without significant loss of accuracy [10]. In general the out of plane deflection z(r,t) can be written as a series of normal modes describing the spanwise deformation

$$z(r,t) = \sum_{k=1}^{\infty} n_k(r) q_k(t) \qquad (4)$$

where n_κ is the mode shape and $q_\kappa(t)$ is the corresponding degree of freedom. For the developed procedure rigid blade motion and the first flapwise bending mode shape, $n=4r^2-3r$, which is appropriate for blade's basic bending deformation can be used alternatively [15].
By these means a detailed rotor induced downwash distribution is obtained by free wake calculations. Sequentially, the blade section angle of attack distribution is computed by

$$\alpha(r,\psi) = \theta(r) - tan^{-1}(u_P/u_T) \qquad (5)$$

where u_P is the air velocity perpendicular to No Feathering Plane (NFP), which includes nonuniform rotor downwash, u_T is the tangential velocity to blade airfoil, both normalized by the rotor tip speed ΩR, and θ(r) is the collective pitch angle (since NFP is taken as reference). With known angle of attack and local velocity, a blade-element type methodology is applied for blade section lift calculations. The above computational procedure is extensively documented in [15].

2.3 Vortex Core Structure

As mentioned above, rotor induced velocity calculation is based on potential field solution such as Biot-Savart law. Due to the absence of viscosity, the induced velocity calculated at a point lying very close to a vortex segment, tends to be infinite which is unrealistic. In order to remove such singularities and model the effects of viscosity in a convenient way the vortex core concept is introduced. A great deal of the current knowledge about the role of viscosity in a vortex core has been derived mainly from experimental measurements. As a result empirical relations are commonly used for the vortex core radius, the velocity distribution at the core region and the viscous core growth.
The core radius is defined as the distance from the core center where the maximum tangential velocity is observed. A corresponding expression for the radial circulation distribution inside the core region is introduced in the computations, which alters the velocity induced from a vortex element. Outside the core region the induced velocity has an approximately potential distribution which tends to coincide with the Biot-Savart distribution fairly away from the vortex line.

Several algebraic models for the vortex induced velocity have been introduced due to their simplicity and computational efficiency in engineering applications [24-26]. According to Vatistas [26] a series of tangential velocity profiles in the vortex core is given by the relation

$$V_\theta(r) = \frac{g\, r}{2\pi\left(r_c^{2n} + r^{2n}\right)^{1/n}} \tag{6}$$

where g is the circulation of the vortex line, n is an integer variable, r is the radial distance from the vortex center and r_c is the core radius. Using this relation for different values of n, the velocity r profiles of some well-known core models can be derived using the nondimensional radius $\bar{r} = r/r_c$ For n=1 the core model suggested by Scully and Sullivan [27] is derived

$$V_\theta(\bar{r}) = \frac{g}{2\pi r_c}\frac{\bar{r}}{(1+\bar{r}^2)} \tag{7}$$

For n=2 the model proposed by Bagai-Leishman in [32] is derived

$$V_\theta(\bar{r}) = \frac{g}{2\pi r_c}\frac{\bar{r}}{\sqrt{1+\bar{r}^4}} \tag{8}$$

Taking these models into account, the present investigation also applies the Rotary Wing vortex model [10] and of the Lamb-Oseen model [28] for the representation of the vortex core structure.

2.4 Core Growth

Unlike airplanes, helicopter rotors remain in close proximity to their tip vortices, more so in descent and maneuvers. This feature leads to close encounters of rotor blades with tip vortices, which as already mentioned are known as blade vortex interactions or BVIs. As a consequence, it is important to understand not only the initial core size after roll-up, but also the subsequent growth of the vortex core [29].

The effect of diffusion on tip vortices is taken into account by increasing the vortex core radius and decreasing its vorticity as time advances. The simplest viscous vortex is the Lamb-Oseen vortex model. This is a two-dimensional flow with circular symmetry in which the streamlines are circles around the vortex filament. The vorticity vector is parallel to the vortex filament and a function of radial distance r and time t. Solving the Navier-Stokes equations for this case an exact solution for the tangential or swirl velocity surrounding the vortex filament arises as

$$V_\theta(r) = \frac{g_{TIP}}{2\pi r}\left(1 - e^{-r^2/4vt}\right) \tag{9}$$

where g_{TIP} is the tip vortex strength and v is the kinematic viscosity. The core growth with time, predicted by the Lamb-Oseen model is given by

$$r_{diff}(t) = 2.24181\sqrt{vt} \tag{10}$$

This result came up by differentiating equation 9 with respect to r and setting the derivative to zero. The Lamb-Oseen vortex can be regarded as the "desingularisation" of the rectilinear line vortex, in which the vorticity has a delta-function singularity.
Squire [30] showed that the solution for a trailing vortex is identical to the Lamb-Oseen solution. So the downstream distance z from the origin of the vortex can be related to time as $t=z/V_4$. In order to account for effects on turbulence generation, Squire introduced an eddy viscosity coefficient δ. In the case of a helicopter rotor, time t is related to the wake age δ_ℓ as $\delta_\ell = \Omega t$, where Ω is the angular velocity of the rotor. Thus, including these parameters equation 10 can be written as

$$r_{diff}(\delta_\ell) = 2.24181\sqrt{\delta v\left(\frac{\delta_\ell + \delta_0}{\Omega}\right)} \tag{11}$$

In the above equation δ_0 is an effective origin offset, which gives a finite value of the vortex core radius at the instant of its generation ($\delta_\ell=0$) equals to

$$r_{diff}(\delta_\ell = 0) \equiv r_0 = 2.24181\sqrt{\delta v\left(\frac{\delta_0}{\Omega}\right)} \tag{12}$$

At this work δ_0 was selected to have an age between 15° and 30°. According to Squire, the eddy viscosity coefficient is proportional to the vortex Reynolds number Re_v and equals to

$$\delta = 1 + a_S\, Re_v \tag{13}$$

where a_s is the Squire's parameter and its value is determined from experimental measurements. A phenomenon often opposing vortex diffusion is the straining of vortex filaments due to their freely distorted geometry. In fact the steep gradients of wake induced velocities cause them to stretch or to squeeze and their core radius to decrease or to increase correspondingly. For straining effects, the following fraction is defined

$$\varepsilon = \frac{\Delta\ell}{\ell} \tag{14}$$

as the strain imposed on the filament over the time interval Δt, where Δℓ is the deformation from its initial length ℓ. Now assume that the filament has a core radius $r_{diff}(\delta_\ell)$ at time δ_ℓ. At time $\delta_\ell+\Delta\psi$ the filament will have a core radius $r_{diff}(\delta_\ell+\Delta\psi)-\Delta r_{diff}(\delta_\ell)=r_{strain}$ because of straining. Applying the principle of conservation of mass leads to the following result

$$r_{strain}(\delta_\ell + \Delta\psi) = r_{diff}(\delta_\ell)\frac{1}{\sqrt{1+\varepsilon}} \tag{15}$$

Combining equations (11) and (15) a vortex core radius including both diffusion and straining effects can be defined as

$$r_c(\delta_\ell) = r_{diff}(\delta_\ell) - r_{strain}(\delta_\ell) = r_{diff}(\delta_\ell) - r_{diff}(\delta_\ell - \Delta\psi)\frac{1}{\sqrt{1+\varepsilon}} \qquad (16)$$

3. RESULTS AND DISCUSSION

Table 1 summarizes the basic parameters of the test cases used at the present work. For all of the test cases the rotor blade radius and the chord length were equal to 2.1 m and 0.14 m respectively.

TABLE 1: Basic parameters of the experimental flight test cases used at the present work.

Test Case	Advance Ratio μ	Tip Path Plane Angle a_{TPP}	Thrust Coefficient C_T	Tip Mach Number M_{TIP}	Type of Flight
1	0.168	6.0°	0.0069	0.616	Ascent
2	0.264	3.0°	0.0071	0.662	Ascent
3	0.166	-1.8°	0.0069	0.617	Descent
4	0.166	-5.7°	0.0070	0.617	Descent

Table 2 shows three different wake models which are compared for the present work. Each of these wake models has been tested with the developed computational procedure and its influence on the rotor aerodynamic forces has been studied.

TABLE 2: Different wake models used for rotor wake simulation.
SLV = Straight Line Vortex, VS = Vortex Sheet

Wake Model	Shed Wake	Inboard Wake	Tip Vortex
1	50 SLV	50 SLV	1 SLV
2	1 SLV	VS	1 SLV
3	VS	VS	1 SLV

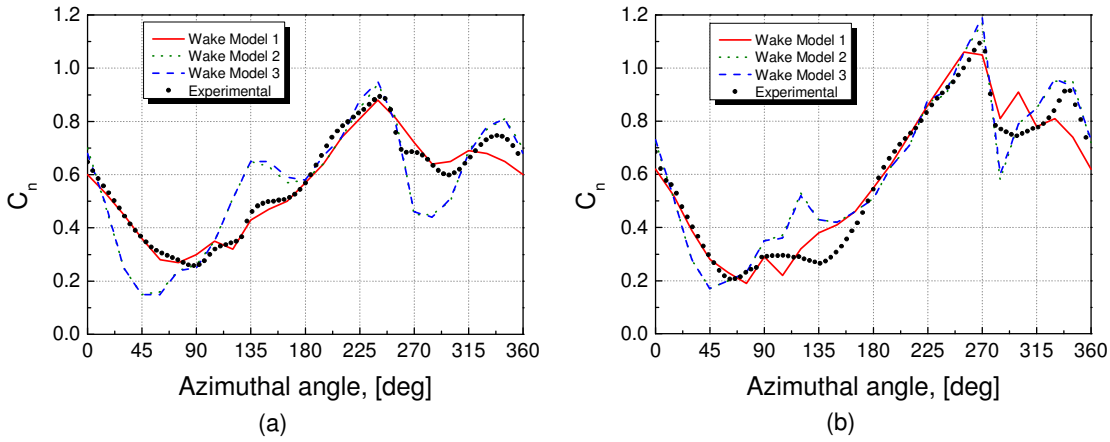

FIGURE 4: Influence of different wake models on the normal force coefficient at radial station 0.82 for two climb cases with different advance ratio, (a) Test Case 1, μ=0.168, (b) Test Case 2, μ=0.268.

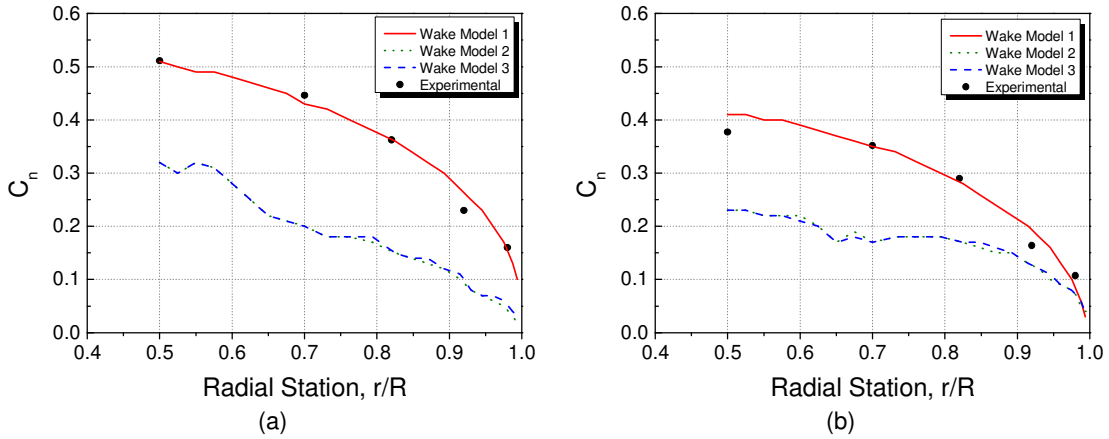

FIGURE 5: Influence of different wake models on the normal force coefficient at azimuth angle $\Psi=45^o$ for two climb cases with different advance ratio, (a) Test Case 1, $\mu=0.168$, (b) Test Case 2, $\mu=0.268$.

In Figure 4 the resulting azimuthal distribution of normal force coefficient C_n is compared with experimental data for the first two test cases of Table 1. For the same test cases the radial distribution of normal force coefficient C_n is compared with experimental data as shown in Figure 5.

It is evident from these figures that representing the total rotor wake with n-straight line vortices is preferable than using vortex sheets for trailing or shed wake. Especially at rotor disk areas where Blade Vortex Interaction phenomena are likely to occur, as for azimuth angles 90^o to 180^o and 270^o to 360^o, wake model 1 gives substantially better results because the existing fluctuations of bound circulation distribution are adequate simulated. For the test cases shown, radial airloads distribution also differs at 45^o where the results of wake model 1 follow closely the experimental values. For this reason wake model 1 is used hereafter.

Another observation is that wake models 2 and 3 give better results by the increment of the advance ratio, which demonstrates that helicopter rotor wake representation could be simpler for high speed flights, saving extra computational time. On the other hand an elaborate rotor wake model is crucial for low speed flights.

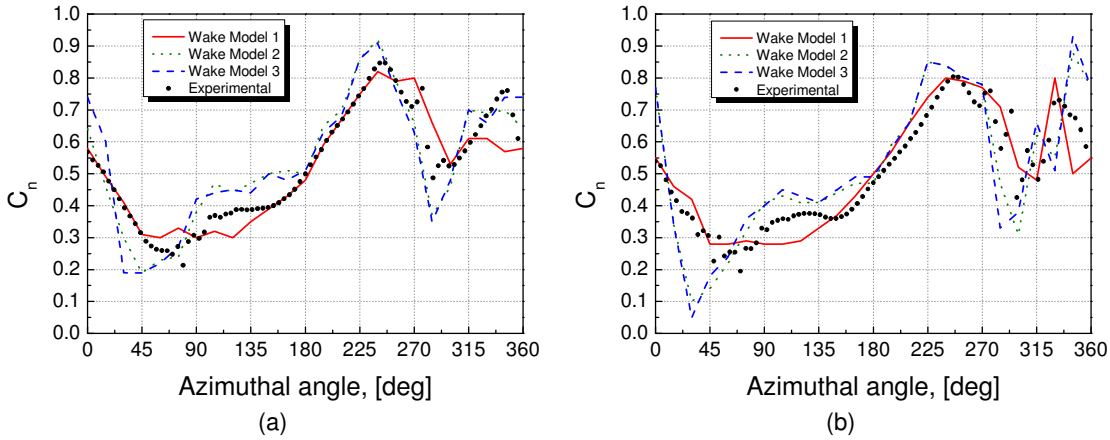

FIGURE 6: Influence of different wake models on the normal force coefficient at radial station 0.82 for two descent cases with different TPP angle, (a) Test Case 3, $a_{TPP}=-1.8^o$, (b) Test Case 4, $a_{TPP}=-5.7^o$.

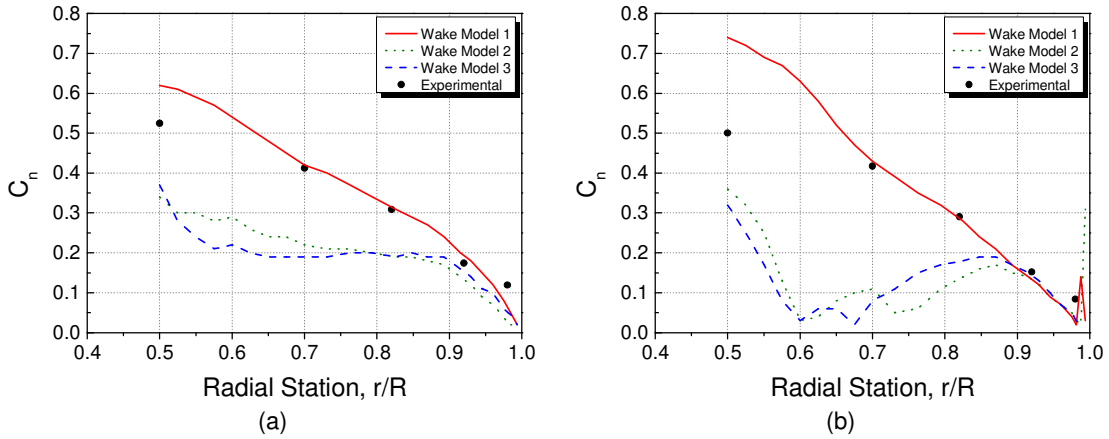

FIGURE 7: Influence of different wake models on the normal force coefficient at azimuth angle $\Psi=45^o$ for two descent cases with different TPP angle, (a) Test Case 3, $a_{TPP}=-1.8^o$, (b) Test Case 4, $a_{TPP}=-5.7^o$.

In Figures 6 and 7 the azimuthal and radial distribution of normal force coefficient respectively is compared with experimental data for test cases 3 and 4 of Table 1. The multiple vortex lines model gave better results than the other two wake models although there is considerable deviation from the experimental data especially for test case 4, where $a_{TPP}=-5.7^o$. This is due to the intensive Blade Vortex Interactions (BVI) occurred at descent flight cases and especially at the specific region of TPP angle, as demonstrated from wind tunnel results [16,23].

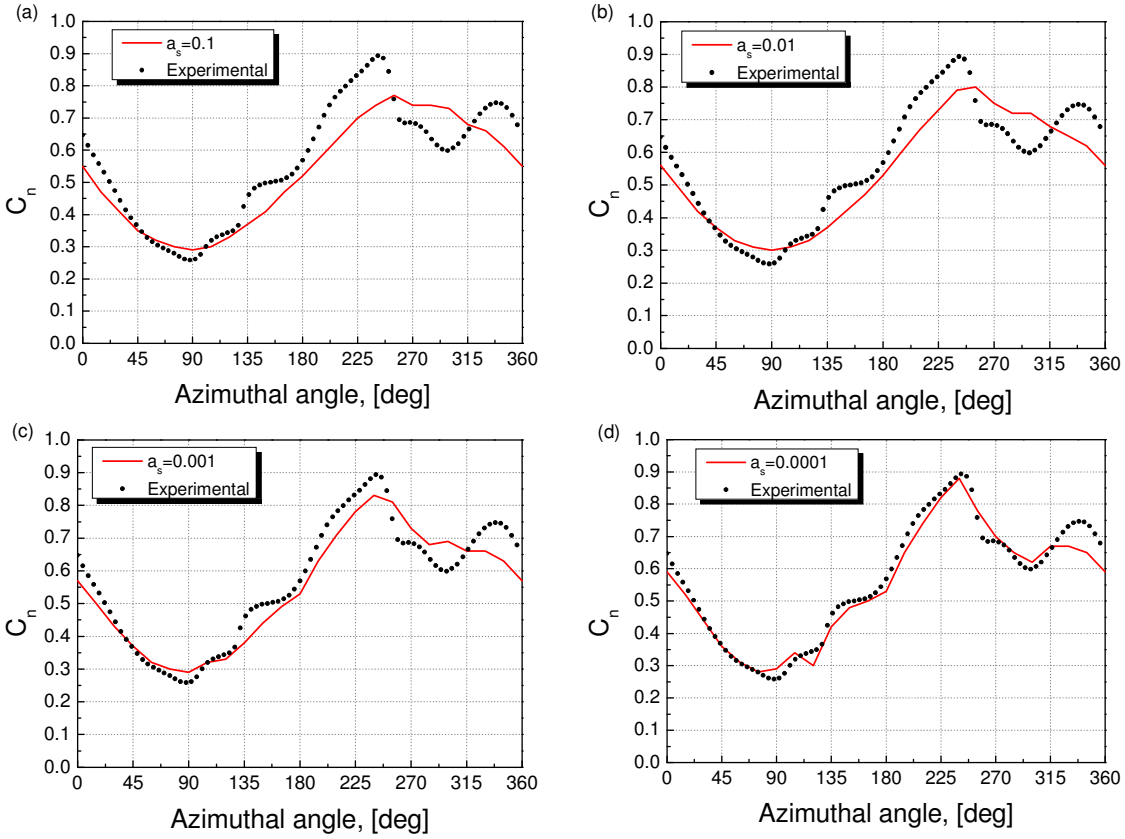

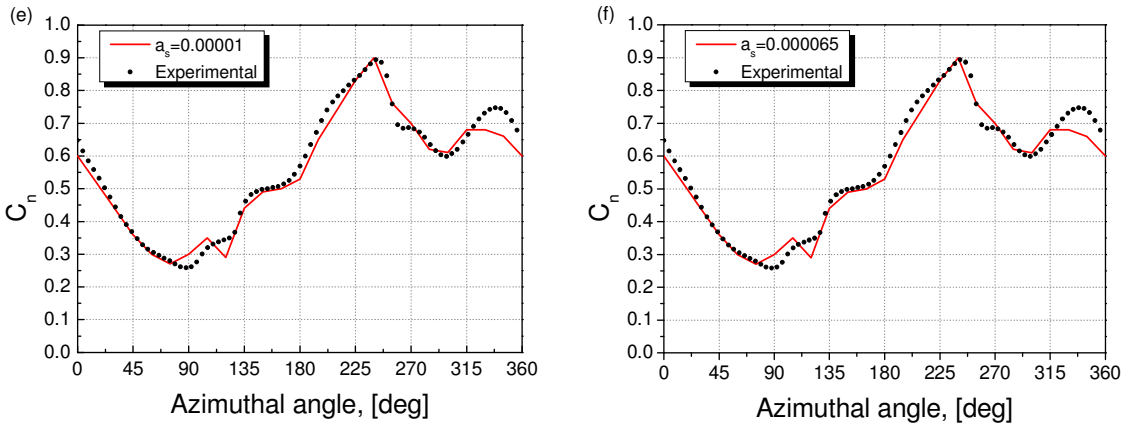

FIGURE 8: Computational investigation for the definition of Squire's parameter a_s. The diagrams correspond to the test case 1 flight conditions.

As mentioned before in order to include diffusion effects in the vortex core, Squire's parameter a_s must be defined. For this purpose a computational investigation has been done for the derivation of an acceptable value of a_s.

Figure 8 shows the azimuthal distribution of the normal force coefficient for several values of a_s varying from 10^{-1} to 10^{-5}. Comparing the computed results with the corresponding experimental ones for test case 1, a value of the order 10^{-4} to 10^{-5}, as indicated in diagrams (d) and (e) in Figure 8, seems to achieve best results. This value for a_s has also been suggested by Leishman [31]. At this work a value of 0.000065 was selected for a_s as shown in the diagram (f) in Figure 8.

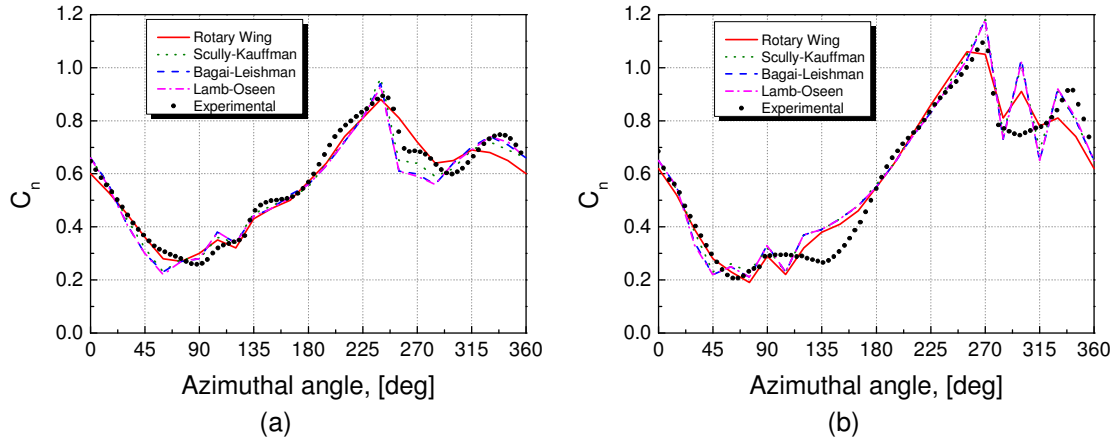

FIGURE 9: Influence of different core models on the normal force coefficient at radial station 0.82 for two climb cases with different advance ratio, (a) Test Case 1, μ=0.168, (b) Test Case 2, μ=0.268.

Having found an appropriate value for a_s, several core models are applied to simulate the tip vortex core structure. In Figures 9 and 10 the azimuthal and radial distribution of normal force coefficient respectively is compared with experimental data for test cases 1 and 2 as presented in Table 1. Four different core models are tested. As expected, Scully-Kauffman, Bagai-Leishman and Lamb-Oseen core models give about the same results. This is due to the fact that these core models were obtained from the same series family proposed by Vatistas. The rotary wing gave better results than the other three core models, demonstrating that this model is suitable for helicopter climb test cases.

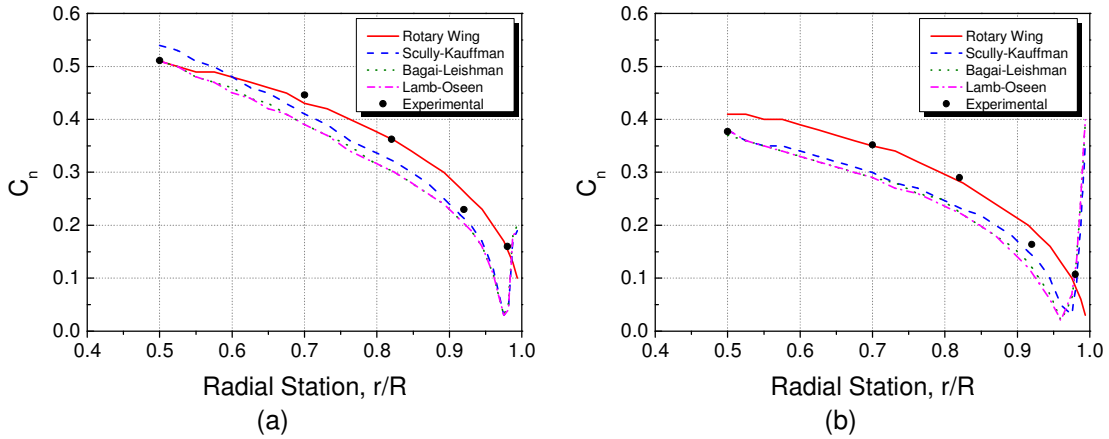

FIGURE 10: Influence of different core models on the normal force coefficient at azimuth angle $\Psi=45^o$ for two climb cases with different advance ratio, (a) Test Case 1, $\mu=0.168$, (b) Test Case 2, $\mu=0.268$.

The same core models were applied for the two descent test cases 3 and 4 (Table 1). As shown in Figure 11 all core models give about the same overall results, underestimating the value of C_n at azimuthal angles between 90^o and 135^o. The three core models which belong to the same series family fit better to the experimental data than the rotary wing, for azimuthal angles between 315^o and 360^o. Also from Figure 12 seems that these models correspond better to the experimental data and especially for the second descent test case, as shown in Figure 12b where intense BVI phenomena occurred as mentioned previously. Due to its simplicity the Scully-Kauffman core model is an option, but in order to include diffusion and straining effects the Lamb-Oseen model is preferable.

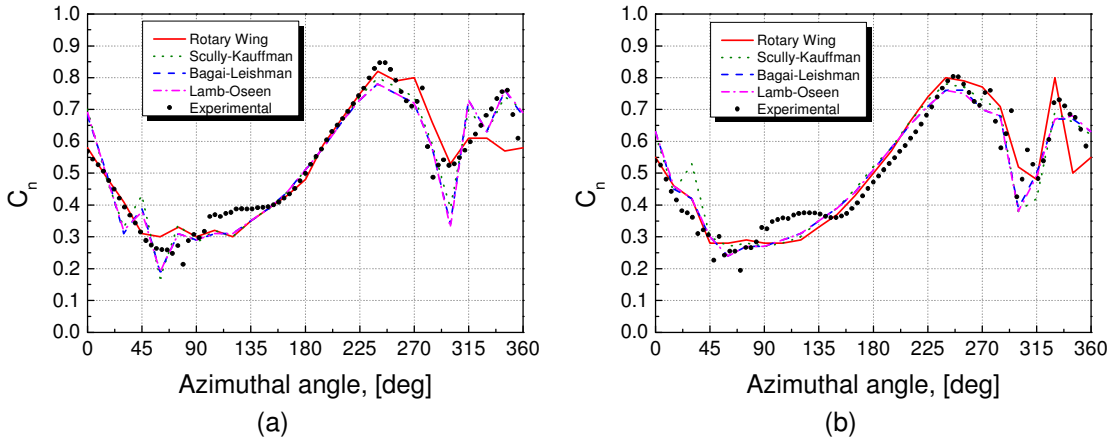

FIGURE 11: Influence of different core models on the normal force coefficient at radial station 0.82 for two descent cases with different TPP angle, (a) Test Case 3, $a_{TPP}=-1.8^o$, (b) Test Case 4, $a_{TPP}=-5.7^o$.

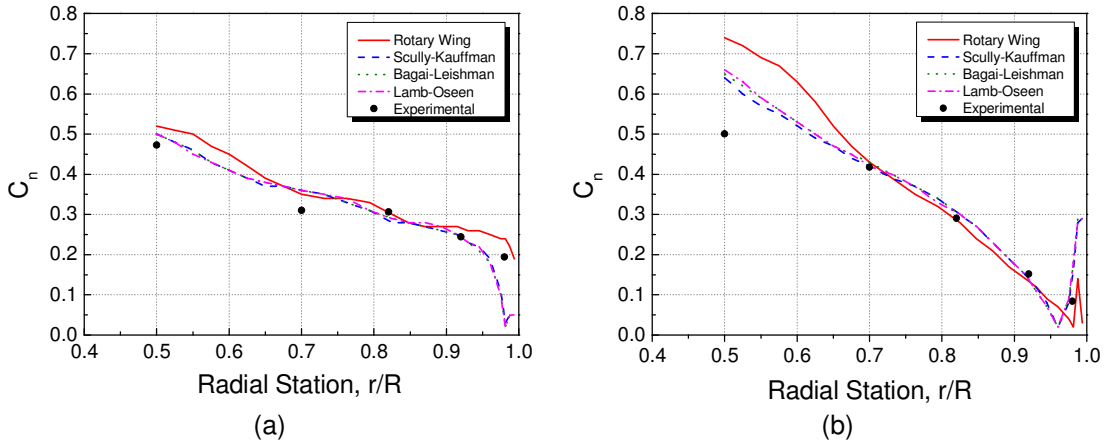

FIGURE 12: Influence of different wake models on the normal force coefficient at azimuth angle $\Psi=45^o$ for two descent cases with different TPP angle, (a) Test Case 3, $a_{TPP}=-1.8^o$, (b) Test Case 4, $a_{TPP}=-5.7^o$.

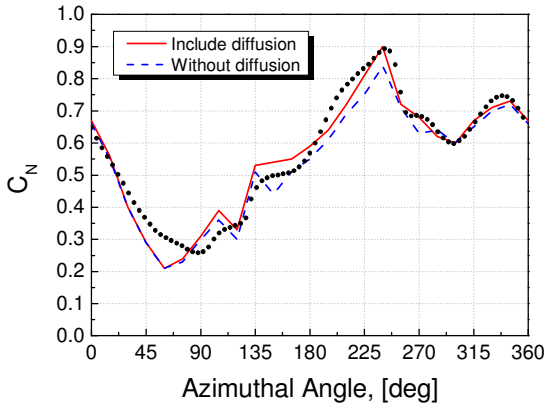

FIGURE 13: Comparison of experimental and computed azimuthal distribution of normal force coefficient C_n for the test case 1 flight conditions, when diffusion effects are included and neglected respectively.

The importance of diffusion effects was also studied. Using the Lamb-Oseen model for the straight line tip vortex core structure, a comparison is made between experimental and computed C_n for the cases where diffusion effects are included and neglected respectively. The diagram in Figure 13 shows that better results can be obtained when diffusion effects are included, although the differences are small.

An effort was also made in order to include straining effects at the tip vortex core growth. This phenomenon is often opposing diffusion as already mentioned. Figure 14 shows the computed azimuthal distribution of C_n for the cases where straining effects are included and neglected respectively. The results are compared with experimental data. For the current test case it seems that straining effects do not play an important role as diffusion.

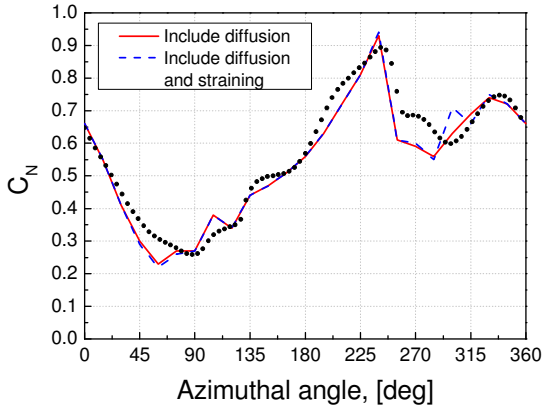

FIGURE 14: Comparison of experimental and computed azimuthal distribution of normal force coefficient C_n for the test case 1 flight conditions, when straining effects are included and neglected respectively.

4. CONSLUSIONS

A computational model for the simulation of helicopter rotor wake has been developed using multiple trailing vortex lines. Diffusion and straining effects of the tip vortex have been appropriate incorporated in order to investigate their influences. To include viscous effects several core models have been tested.

The conclusions from this study are summarized as follows:

1. Despite the extra computational cost, simulating the rotor wake by multiple trailing vortex lines is preferable than using vortex sheets for the inboard or the shed wake. This is crucial especially for low speed helicopter flight.
2. In order to include diffusion effects, Squire's parameter a_s has been found to be of the order of 10^{-4} to 10^{-5}. At this work a value equal to 0.000065 was selected.
3. The rotary wing core model seems to be more suitable for helicopter climb flight cases.
4. For descent flight cases, where intense BVI phenomena occurred, the Lamb-Oseen core model is preferable due to its ability to include diffusion and straining effects. The Scully-Kauffman core model is an option because of its simplicity.
5. Diffusion effects are important on the calculation of helicopter rotor aerodynamic forces, but straining effects do not influence computational results as much as diffusion.

5. REFERENCES

1. W. Johnson. "*Rotorcraft aerodynamics models for a comprehensive analysis"*. Proceedings of 54th Annual Forum of American Helicopter Society, Washington, DC, May 20-22, 1998.
2. G. J. Leishman, M. J. Bhagwat and A. Bagai. "*Free-vortex filament methods for the analysis of helicopter rotor wakes"*. Journal of Aircraft, 39(5):759-775, 2002.
3. T. A. Egolf and A. J. Landgrebe. "*A prescribed wake rotor inflow and flow field prediction analysis"*. NASA CR 165894, June 1982.
4. T. S. Beddoes. "*A wake model for high resolution airloads*". Proceedings of the 2nd International Conference on Basic Rotorcraft Research, Univ. of Maryland, College Park, MD, 1985.
5. M. J. Bhagwat and G. J. Leishman. "*Stability, consistency and convergence of time-marching free-vortex rotor wake algorithms*". Journal of American Helicopter Society, 46(1):59-71, 2001.
6. T. R. Quackenbush, D. A. Wachspress and Boschitsch. "*Rotor aerodynamic loads computation using a constant vorticity contour free wake model*". Journal of Aircraft, 32(5):911-920, 1995.
7. K. Chua and T.R. Quackenbush. "*Fast three-dimensional vortex method for unsteady wake calculations*". AIAA Journal, 31(10):1957-1958, 1993.

8. M. J. Bhagwat and G. J. Leishman. "*Rotor aerodynamics during manoeuvring flight using a time-accurate free vortex wake*". Journal of American Helicopter Society, 48(3):143-158, 2003.
9. G. H. Xu and S. J. Newman. "*Helicopter rotor free wake calculations using a new relaxation technique*". Proceedings of 26th European Rotorcraft Forum, Paper No. 37, 2000.
10. M. P. Scully. "*Computation of helicopter rotor wake geometry and its influence on rotor harmonic airloads*". ASRL TR 178-1, 1975
11. A. J. Chorin. "*Computational fluid mechanics*". 1st edition, Academic Press, (1989).
12. T. Leonard. "*Computing three dimensional incompressible flows with vortex elements*". Annual Review of Fluid Mechanics, 17: 523-559, 1985.
13. T. Sarpkaya. "*Computational methods with vortices - The 1988 Freeman scholar lecture*". ASME Journal of Fluids Engineering, 111(5):5-52, March 1989.
14. N. Hariharan and L. N. Sankar. "*A review of computational techniques for rotor wake modeling*". Proceedings of AIAA 38th Aerospace Sciences Meeting, AIAA 00-0114, Reno NV, 2000.
15. A. I. Spyropoulos, A. P. Fragias, D. G. Papanikas and D. P. Margaris. "*Influence of arbitrary vortical wake evolution on flowfield and noise generation of helicopter rotors*". Proceedings of the 22nd ICAS Congress, Harrogate, United Kingdom, 2000.
16. A. I. Spyropoulos, C. K. Zioutis, A. P. Fragias, E. E. Panagiotopoulos and D. P. Margaris. "*Computational tracing of BVI phenomena on helicopter rotor disk*". International Review of Aerospace Engineering (I.RE.AS.E), 2(1):13-23, February 2009.
17. D. B. Bliss, M. E. Teske and T. R. Quackenbush. "*A new methodology for free wake analysis using curved vortex elements*". NASA CR-3958, 1987.
18. S. Gupta and G. J. Leishman. "*Accuracy of the induced velocity from helicoidal vortices using straight-line segmentation*". AIAA Journal, 43(1):29-40, 2005.
19. D. H. Wood and D. Li. "*Assessment of the accuracy of representing a helical vortex by straight segments*". AIAA Journal, 40(4):647-651, 2005.
20. M. Ramasamy, G. J. Leishman. "*Interdependence of diffusion and straining of helicopter blade tip vortices*". Journal of Aircraft, 41(5):1014-1024, 2004.
21. C. Tung and L. Ting. "*Motion and decay of a vortex ring*". Physics of Fluids, 10(5):901-910, 1967.
22. J. A. Stott and P. W. Duck. "*The effects of viscosity on the stability of a trailing-line vortex in compressible flow*". Physics of Fluids, 7(9):2265-2270, 1995.
23. W. R. Splettstoesser, G. Niesl, F. Cenedese, F. Nitti and D. G. Papanikas. "*Experimental results of the European HELINOISE aeroacoustic rotor test*". Journal of American Helicopter Society, 40(2):3-14, 1995.
24. S. E. Windnall and T. L. Wolf. "*Effect of tip vortex structure on helicopter noise due to blade vortex interactions*". AIAA Journal of Aircraft, 17(10):705-711, 1980.
25. J. M. Bhagwat and G. J. Leishman. "*Correlation of helicopter rotor tip vortex measurements*". AIAA Journal, 38(2):301-308, 2000.
26. G. H. Vatistas, V. Kozel and W. C. Mih. "*A simpler model for concentrated vortices*". Experiments in Fluids, 11(1):73-76, 1991.
27. M. P. Scully and J. P. Sullivan. "*Helicopter rotor wake geometry and airloads and development of laser Doppler velocimeter for use in helicopter rotor wakes*". Massachusetts Institute of Technology Aerophysics Laboratory Technical Report 183, MIT DSR No. 73032, 1972.
28. G. K. Batchelor, "*Introduction to fluid dynamics*". Cambridge University Press, (1967).
29. C. K Zioutis, A. I. Spyropoulos, D. P. Margaris and D. G. Papanikas. "*Numerical investigation of BVI modeling effects on helicopter rotor free wake simulations*". Proceedings of the 24th ICAS Congress, 2004, Yokohama, Japan.
30. H. B. Squire. "*The growth of a vortex in turbulent flow*". Aeronautical Quarterly, 16(3):302-306, 1965.
31. J. M. Bhagwat and G. J. Leishman. "*Generalized viscous vortex model for application to free-vortex wake and aeroacoustic calculations*". Proceedings of American Helicopter Society 58th Annual Forum and Technology Display, Montreal, Canada, 2002.

32. G. J. Leishman, A. Baker and A. Coyne *"Measurements of rotor tip vortices using three-component laser doppler velocimetry"*. Journal of American Helicopter Society, 41(4):342-353, 1996.
33. C. Golia, B. Buonomo and A. Viviani. "*Grid Free Lagrangian Blobs Vortex Method with Brinkman Layer Domain Embedding Approach for Heterogeneous Unsteady Thermo Fluid Dynamics Problems".* International Journal of Engineering, 3(3):313-329, 2009.